

Vessel-Fender Contact Force Modelling for a Real-time Ship Manoeuvring Simulator

F.M. Moreno, H.A.U. Sasaki, H.S. Makiyama & E.A. Tannuri
University of São Paulo, São Paulo, Brasil

ABSTRACT: This paper presents the development of a method for calculating the horizontal contact forces between two bodies in a real-time ship manoeuvring simulator. The method was implemented in the simulator of the University of São Paulo, whose computing core is named "Dyna". The model proposed calculates restoration and friction forces between bodies and has a Momentum-Impulse based criterion to reduce numerical issues when the simulation numerical integration has large time-steps. The model was empirically evaluated at the simulator by deck officers, in real-time simulations with pilots and tugmasters. We also ran simulations of that model to compare its performance under different integration time-steps lengths.

1 INTRODUCTION

Manoeuvring simulations are a crucial tool for evaluating the safety and viability of operations carried at the sea without exposing personnel or assets to risk. On a manoeuvring simulator, the simulated operations can vary widely from navigation in access channels to underway ship-to-ship offloading. In this context, a maritime simulator must incorporate elements usually found in those scenarios and simulate the operation and behaviour of the vessels with sufficient realism.

To achieve the required level of realism, a numerical simulator integrates, in real-time, a complex mathematical model. The numerical simulator computes the floating body dynamics considering hydrodynamic effects and interactions between the vessels and simulated elements such as mooring lines and environmental forces.

One of such interaction is the contact between bodies, for example, between a vessel and the marine fenders in a berth or when a tugboat pushes a ship to

bring it closer to the final position. This physical interaction is complex and depends on the mutual deformation of the bodies and surface interactions (friction). To incorporate such phenomenon in the simulation, a simplified model of the contact is needed.

The modelling of marine fenders and its interactions with vessels and other structures is a vast field, encompassing materials science, analysis made by numerical and empirical models, and optimization of fender properties.

Some research sources provide simplified analytical or empirical approaches for calculating fender forces and other useful parameters [1-2]. Those approaches are usually focused in providing tools for dimensioning piers, berths and the fenders themselves.

Other works focus on the calculus and optimization of fender properties, such as energy absorption, restitution coefficients, etc. by the use of finite element analysis and other numerical models

for solving the deformable body equations [3-5]. Despite being valuable tools, this approach is currently unpractical for Real-Time applications due to the computational costs required.

This paper presents a contact force model developed and implemented in a Real-Time Ship Manoeuvring Simulator. The model separates the contact forces into restoration and friction forces. It adopts a Momentum-Impulse balance criterion to allow its use in a numerical simulator with large time-step integration without numerical issues.

The next section provides an overview of the proposed Contact Engine, section 3 explains the model implemented, section 4 compares the model behaviour for different time-step integrations, and section 5 presents the conclusion.

2 OVERVIEW

The proposed model was developed for the TPN Ship Manoeuvring Simulation Center. That simulator adopts a 6-DoF mathematical model (TPN-MM) based on a long-term experience in ship hydrodynamics. Besides, the TPN-MM follows ITTC procedures to calibrate and validate manoeuvring models. The TPN-MM is based on a quasi-explicit heuristic model for estimating manoeuvring forces on ships. It also comprises models for environmental forces (wind, current, waves), restricted water effects (bottom and bank interaction) and external forces (cables, vector tugboats). The numerical code has been described in detail in the references [6]. It can also incorporate forces provided by external programs, such as the Contact Engine presented in this paper.

Despite the Manoeuvring Simulator having 6 DoF, the proposed Contact Engine considers only forces and geometries of contacting bodies in the 3 DoF horizontal plane. This approach was adopted to simplify the model and reduce computational cost without compromising the realism of the simulation, since vertical contacting forces are negligible during regular operations.

That 2D Contact Engine should provide as output the contact forces that will be integrated in the dynamical simulation with a time-step of $\Delta t=0.1s$ second by forward Euler. The Contact Engine receives as inputs the 2D geometric shape of the objects in the simulation scenario, their current positions and velocities, and the physical contact parameters defined by the user. An overview of the process is shown in the flowchart in Figure 1.

3 METHODOLOGY

This section explains the simplified method adopted for calculating the interaction force between two objects. The next subsections, from 3.1 through 3.3, explain how the forces are calculated. Section 3.4 describes how an impulse-momentum heuristic is applied to limit the calculated forces in order to avoid numerical issues.

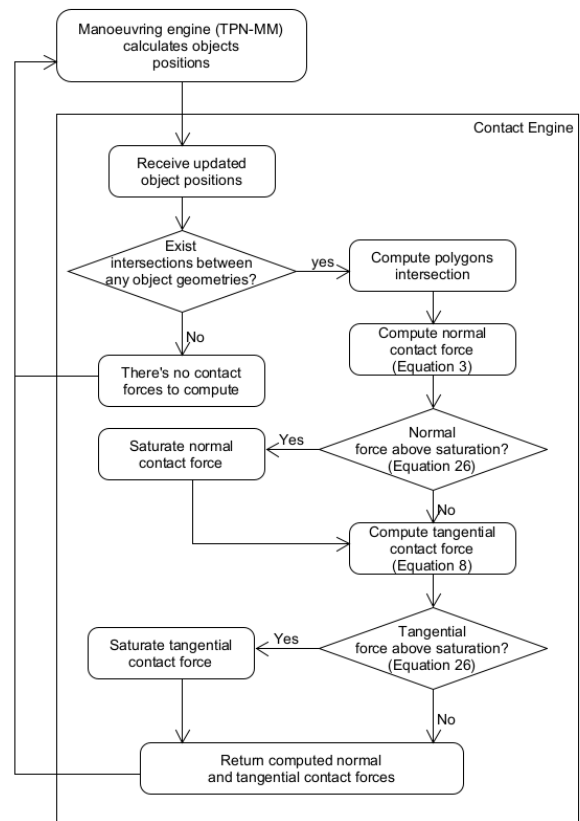


Figure 1. Flowchart of the process for computing contact forces in the Contact Engine and how it interacts with the numerical simulator

3.1 Definitions

The model considers the contacting objects as being 2D convex polygons in the horizontal plane OXY (Figure 2) which have positions and velocities defined externally by the manoeuvring simulator. Each object represents a vessel, harbour fender or another port element. The model is defined in discretized time, and it runs with the same time-step of the manoeuvring simulator ($\Delta t=0.1s$). From here on, the superscript n will be used to denote the time-step of the variables and the subscript pair i,j will denote that the variable is respective to object j and the direction i .

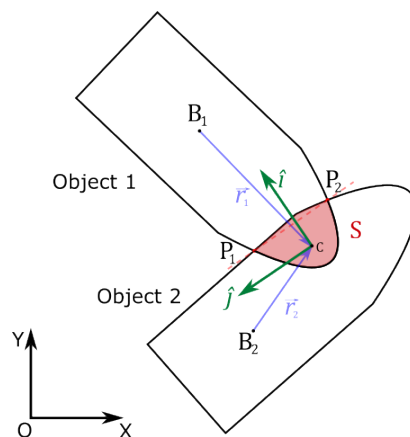


Figure 2. Definition of components obtained from the contact between two objects. It is also worth noticing that under normal circumstances, the intersection area A is much smaller than the one depicted in the Figures in this work.

The contact happens when there is an intersection between two object polygons. The contact polygon S is defined as the intersection between the projected area of the colliding objects in the plane OXY and its centroid being defined as C (Figure 2). It is also defined the vector r_j as the distance of the C point from the barycentre of each object B_j .

The intersection of the two polygon edges also produces two intersection points (P_1 and P_2) that are used to define a “contact line” between the bodies (Figure 1b). The contact line is used to define a local base oxy , with origin in C , with axis $x \perp P_1P_2$ and $y \parallel P_1P_2$, and unitary vectors \hat{i} and \hat{j} respectively.

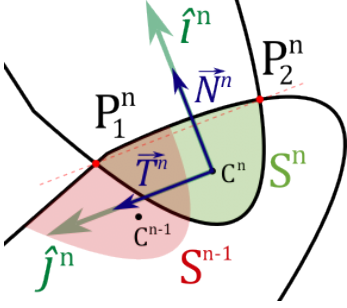


Figure 3. Intersection points and “contact line” (red dotted line) and contact basis oxy for the time-step n

These definitions are kept as the system evolves in time. The contact forces are divided into two components, a normal one N^n and a tangential one T^n and both have their direction set as $\bar{N}^n \cdot \hat{j}^n = 0$ and $\bar{T}^n \cdot \hat{i}^n = 0$ respectively, as shown in Figure 3.

As these forces are equally applied in the two bodies by the third Newton’s Law (Figure 4) [1], the following relation (Equation (1)) can be established:

$$\bar{F}_i^n = -\bar{F}_j^n, \quad \text{with} \begin{cases} F = \{T, N\} \\ i, j = 1, 2 \end{cases} \quad (1)$$

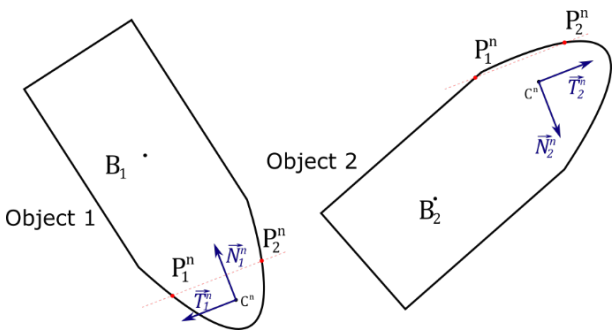


Figure 4. Forces applied on both objects in time-step n . Force is applied at the point C^n .

We assume that forces in the \hat{i} direction are provoked by elastic deformation of the bodies, and forces in the \hat{j} direction are due to friction between the bodies. We will consider that the contact forces are solely applied in the point C on both objects.

Each object is considered a rigid body and has an associated mass m_j and rotational inertia I_j around the body barycentre B_j . The mass m_j is the sum of both inertial and added mass in the OXY directions. Since the value of added mass changes with the

direction of acceleration, only the smallest value is considered in m_j . In cases of harbour fenders or other fixed objects, we consider that $m_j \rightarrow \infty$ and $I_j \rightarrow \infty$.

3.2 Normal Contact Model

The model’s normal forces are obtained from a spring-dampener model defined in equation (2), where k is an area stiffness and c is a damping coefficient. The model is discretized in time by a first-order, backward finite difference, thus obtaining the equation (3). The dot product is defined by the operator (\cdot) and $\text{sgn}(\cdot)$ is the sign function.

$$\bar{N}_j(t) = - \left(k \cdot S(t) - c \cdot \frac{dS(t)}{dt} \right) \text{sgn}(\bar{r}_j(t) \cdot \hat{i}(t)) \cdot \hat{i}(t) \quad (2)$$

$$\bar{N}_j = - \left(k \cdot S^n - c \cdot \frac{S^n - S^{n-1}}{\Delta t} \right) \text{sgn}(\bar{r}_j^{n-1} \cdot \hat{i}^n) \cdot \hat{i}^n \quad (3)$$

3.3 Tangential Contact Model

Regarding the calculation of the tangential force \bar{T}^n , the collision polygon was considered a soft fender, as exemplified in Figure 5a. This soft fender is held in the second body by friction forces in a reference point P_f , and it can be sheared if there is relative movement between the vessels in the \hat{j}^n direction, as shown in Figure 5b. The amount of Shearing, or lateral displacement, is defined as Δs^n .

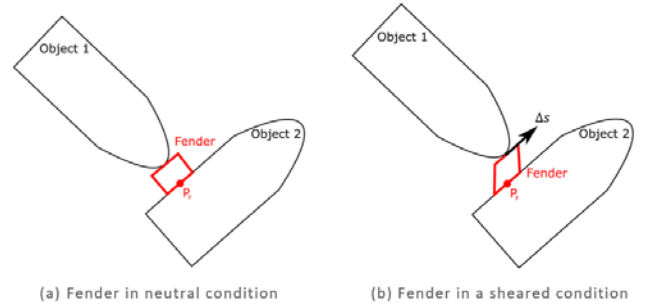


Figure 5. Fender model representation. The fender can be sheared if there is relative motion between contacting objects.

That shearing produces a restoration force that tends to force both objects to return to their initial relative positions in the \hat{j}^n direction. The magnitude of those restoration forces is proportional to both the shearing of the fender in the \hat{j}^n direction (Δs^n), and a shearing stiffness k_s , as shown in equation (4).

$$\bar{T}_1^n = -k_s \Delta s^n \hat{j}^n \quad (4)$$

Equation (4) is valid if there is no sliding between the fender and the contacting object in the time-step n . We can consider that there is no sliding if the static friction force is enough to counteract \bar{T}_i . This condition is satisfied when the inequality in equation

(5) is satisfied, where μ_s is the coefficient of static friction between the object and the fender.

$$k_s |\Delta s^n| \leq \left\| \bar{N}_j^n \right\| \mu_s \quad (5)$$

If the restoration forces are larger than the static friction force, then the fender slides in the direction of Δs^n . If there is sliding, the restoration force is limited by the dynamic friction force defined in equation (6), where μ_k is the coefficient of dynamic friction between the object and fender.

$$\bar{T}_1^n = - \left\| \bar{N}_j^n \right\| \mu_k \operatorname{sgn}(\Delta s^n) \quad (6)$$

We consider that when the fender slides in one time-step it will slide enough to achieve equilibrium in the next time-step (Figure 6). Thus, in the next time-step, we update the contact point considering a residual fender shearing that is enough to equilibrate the dynamic friction, as defined in equation (7).

$$k_s \Delta s^{n+1} = \left\| \bar{N}_j^n \right\| \mu_k \operatorname{sgn}(\Delta s^n) \Rightarrow \frac{\left\| \bar{N}_j^n \right\| \mu_k}{k_s} \operatorname{sgn}(\Delta s^n) \quad (7)$$

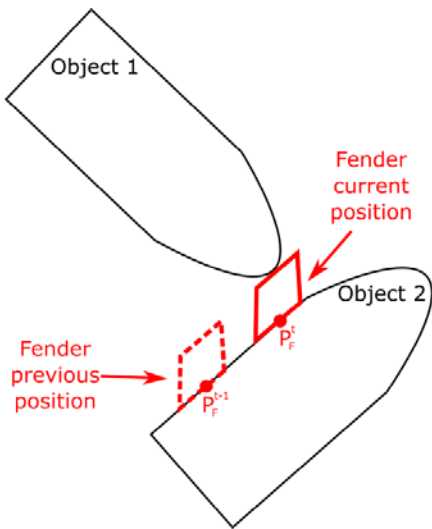


Figure 6: Fender sliding along the contact line. The sliding happens in one time-step and the fender is still sheared after the sliding stops.

We can summarize the fender behaviour in equation (8), where the fender has two states depending on the amount of shearing force: for small enough displacements, the fender point P_F is kept fixed in the object by static friction, while for larger displacements, it slides along the contact line.

$$\begin{cases} \bar{T}_1^n = -k_s \Delta s^n \hat{j}^n & \text{if } \Delta s^t \leq \frac{\mu_s \left\| \bar{N}_j^n \right\|}{k_s} \text{ (NoSliding)} \\ \bar{T}_1^n = - \left\| \bar{N}_j^n \right\| \mu_k \operatorname{sgn}(\Delta s^n) & \text{if } \Delta s^t > \frac{\mu_s \left\| \bar{N}_j^n \right\|}{k_s} \text{ (Sliding)} \\ \Delta s^{n+1} = \operatorname{sgn}(\Delta s^n) \left\| \bar{N}_j^{n+1} \right\| \frac{\mu_k}{k_s} \end{cases} \quad (8)$$

To apply that fender model to our collision model, we need a heuristic to calculate the lateral displacement Δs^n . We achieve this by following the steps below:

1. We define the lateral displacement at the start of the contact as zero ($\Delta s^0=0$).
2. While there is contact between the bodies:
 - Consider two points coincident to C^n that are individually fixed in objects 1 and 2 at the time-step $n=T \geq 0$, here denominated C_1^T, C_2^T .
 - At the time-step $n=T+1$ we compare how much C_1^T moved in relation to C_2^T (Figure 7) along the direction of \hat{j}^{n+1} and add the value to Δs^T , following the formula $\Delta s^{T+1} = \Delta s^T + (C_2^T - C_1^T) \cdot y^{T+1}$.
 - If there was sliding in the previous time-step, $n=T$, define Δs^{T+1} accordingly to equation (8).

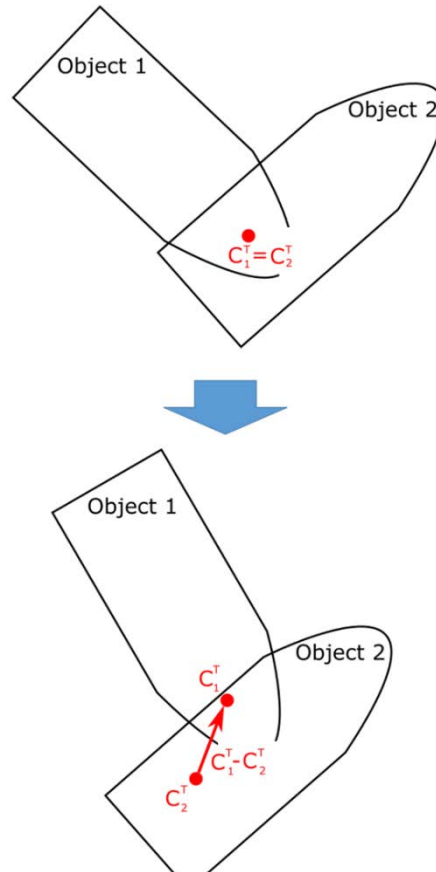


Figure 7: Depiction of how the amount of fender shear is computed in our model, the point C^T is fixed in both objects at one time-step, then the amount of displacement between those points in the next time-step is used as basis for the computation fender shear.

3.4 Impulse-Momentum Approach for Limiting Contact Forces

In situations where the contact between objects has high stiffness (large k), or the relative velocity between objects is large, there is the potential to emerge unrealistic large contact forces that will produce numerical issues unless a very small integration time-step is used. In order to avoid such issues in the simulator, we use an Impulse-Momentum heuristic to limit those contact forces.

We consider that the contact is a partially elastic collision [1]. Therefore, after the contact, the objects will have a relative velocity that is at most a fraction of the relative velocity at the start of the contact, as defined by (9). In this equation, \overline{VC}_x^0 is the initial relative velocity in the i^0 direction, \overline{VC}_y^0 is the initial relative velocity in the j^0 direction, γ is the restitution coefficient of the contact, and \overline{VC}_x^{final} and \overline{VC}_y^{final} are the relative velocities at the end of the contact between objects.

$$\begin{cases} \overline{VC}_x^{final} \leq -\gamma \overline{VC}_x^0 \\ \overline{VC}_y^{final} \leq -\gamma \overline{VC}_y^0 \end{cases} \quad (9)$$

The relative velocities \overline{VC}_x^n and \overline{VC}_y^n are defined as the difference between the instantaneous velocities of points C_1^n and C_2^n , as shown in equation (10), where $\overline{V}_{C_1}^n$ is the absolute velocity of the point C_1^n , and $\overline{V}_{C_2}^n$ is the absolute velocity of the point C_2^n .

$$\begin{cases} \overline{VC}_x^n = (\overline{V}_{C_1}^n - \overline{V}_{C_2}^n) \cdot \hat{i}^n \\ \overline{VC}_y^n = (\overline{V}_{C_1}^n - \overline{V}_{C_2}^n) \cdot \hat{j}^n \end{cases} \quad (10)$$

One way to guarantee that the inequalities in equation (9) are satisfied is to limit the change of velocity in one time-step to a value that will not make the velocity in the next time-step violate those inequalities. From now on we will adopt that criterion, described in equation (11), where the delta operator (Δ) denotes the variation in the quantity from the current time-step to the previous.

$$\begin{cases} \Delta \overline{VC}_x^{n+1} = \overline{VC}_x^n - \gamma \overline{VC}_x^0 \\ \Delta \overline{VC}_y^{n+1} = \overline{VC}_y^n - \gamma \overline{VC}_y^0 \end{cases} \quad (11)$$

And by applying the delta operator to equation (10) we can relate the change in relative velocity $\Delta \overline{VC}_i^{n+1}$ to the change of velocity of points $\overline{V}_{C_1}^n$ and $\overline{V}_{C_2}^n$ as shown in equation (12).

$$\begin{cases} \Delta \overline{VC}_x^{n+1} = (\Delta \overline{V}_{C_1}^n - \Delta \overline{V}_{C_2}^n) \cdot \hat{i}^n \\ \Delta \overline{VC}_y^{n+1} = (\Delta \overline{V}_{C_1}^n - \Delta \overline{V}_{C_2}^n) \cdot \hat{j}^n \end{cases} \quad (12)$$

The relation between the change in velocity and the applied force is defined by the Impulse-Momentum balance equations (13) [1], where the first

equation links the linear velocity variation of the body barycentre ($\overline{\Delta v}_{B_j}$) with the sum of applied forces in the body ($\sum \overline{F}_j$) and the second one links the angular velocity ($\overline{\Delta \omega}_j$) with the sum of applied torques ($\sum \overline{\tau}_j$). m is the mass and I is the moment of inertia of the body. Δt is the duration of the application of force or torque. The applied torque and moment of inertia are referent to the body barycentre.

$$\begin{cases} m_j \overline{\Delta v}_{B_j} = \sum \overline{F}_j \Delta t \\ I_j \overline{\Delta \omega}_j = \sum \overline{\tau}_j \Delta t \end{cases} \quad (13)$$

To use equation (13), we must link the relative velocities between objects and the velocities of the objects barycentre. This can be achieved by considering that both objects are rigid bodies, so we can obtain the $\overline{V}_{C_j}^n$ velocities from the velocities of the objects at their barycentre ($\overline{V}_{B_j}^n$), plus their angular velocities, $\overline{\omega}_j^n$, and the arm vector that connects the C^n to the object respective barycentre r_j^n (as in Figure 2), by using the rigid body formula (14) [2].

$$\overline{V}_{C_j}^n = \overline{V}_{B_j}^n + \overline{\omega}_j^n \times r_j^n \quad (14)$$

We can define that the variation of $\overline{V}_{C_j}^n$ and $\overline{V}_{C_j}^{n+1}$ from one time-step to the next depends on the changes of barycentre ($\overline{v}_{B_j}^n$) and angular velocity ($\overline{\omega}_j^n$) as shown in equation (15). For simplicity, we assume that the vectors r_j^n are kept almost constant from one time-step to the next.

$$\Delta \overline{V}_{C_j}^{n+1} = \overline{V}_{C_j}^{n+1} - \overline{V}_{C_j}^n = \Delta \overline{V}_{B_j}^{n+1} + \Delta \overline{\omega}_j^{n+1} \times r_j^n \quad (15)$$

Considering the Impulse-Momentum balance equation (13), we can rewrite the rigid body equation (14) and obtain the equation (16), considering the normal and parallel contact forces acting on the object.

$$\Delta \overline{V}_{C_j}^{n+1} = \Delta \overline{V}_{B_j}^{n+1} + \Delta \overline{\omega}_j^{n+1} \times r_j^n = \frac{(\overline{T}_j^n + \overline{N}_j^n)}{m_j} \Delta t + \frac{\sum \overline{\tau}_j^n}{m_j} \Delta t \times r_j^n \quad (16)$$

The sum of contact torques applied on object 1 ($\sum \overline{\tau}_1$) can be obtained from the sum of contact forces and the arm between C_A and the object barycentre, as shown in equation (17):

$$\sum \overline{\tau}_j^n = r_j^n \times (\overline{T}_j^n + \overline{N}_j^n) \quad (17)$$

And by substituting equation (17) on (16) we obtain equation (18):

$$\Delta \overline{V}_{C_j}^{n+1} = \frac{(\overline{T}_j^n + \overline{N}_j^n)}{m_j} \Delta t + \frac{r_j^n \times (\overline{T}_j^n + \overline{N}_j^n)}{I_j} \times r_j^n \Delta t \quad (18)$$

By applying the vector triple product, it is possible to decompose the cross product in equation (18) and obtain equation (19):

$$\Delta \overline{V}_{C_j}^{n+1} = \frac{(\overline{T}_j^n + \overline{N}_j^n)}{m_j} \Delta t + \frac{\Delta t}{I_j} \left(\left\| \overline{r}_j^n \right\|^2 (\overline{T}_j^n + \overline{N}_j^n) - \overline{r}_j^n \cdot (\overline{T}_j^n + \overline{N}_j^n) \overline{r}_j^n \right) \quad (19)$$

And by decomposing the change in velocity $\Delta \overline{V}_{C_j}^{n+1}$ in equation (19) into \hat{i}^n and \hat{j}^n components we obtain equation (20):

$$\begin{cases} \Delta \overline{V}_{C_{j,x}}^{t+1} = \frac{(\overline{N}_j^n)}{m_j} \Delta t + \frac{\Delta t}{I_j} \left(\left\| \overline{r}_j^n \right\|^2 (\overline{N}_j^n) - (\overline{r}_j^n \cdot (\overline{T}_j^n + \overline{N}_j^n)) (\overline{r}_j^n \cdot \hat{i}^n) \right) \\ \Delta \overline{V}_{C_{j,y}}^{t+1} = \frac{(\overline{T}_j^n)}{m_j} \Delta t + \frac{\Delta t}{I_j} \left(\left\| \overline{r}_j^n \right\|^2 (\overline{T}_j^n) - (\overline{r}_j^n \cdot (\overline{T}_j^n + \overline{N}_j^n)) (\overline{r}_j^n \cdot \hat{j}^n) \right) \end{cases} \quad (20)$$

The equation (20) associates the change in velocity with the collision forces, but the presence of both \overline{T}_j^n and \overline{N}_j^n in the same equation poses a problem, since no explicit formula can be obtained for all cases. The solution adopted in this work considers that the forces normal to the contact line are higher than the parallel forces ($\overline{N}_j^n \gg \overline{T}_j^n$), so the equation for the $\Delta \overline{V}_{C_j}^{n+1}$ component can be simplified by discarding the \overline{T}_j^n force, as shown in equation (21):

$$\begin{aligned} \Delta \overline{V}_{C_j}^{n+1} &= \frac{\overline{N}_j^n \Delta t}{m_j} + \frac{\Delta t}{I_j} \left(\left\| \overline{r}_j^n \right\|^2 \overline{N}_j^n - (\overline{r}_j^n \cdot \overline{N}_j^n) (\overline{r}_j^n \cdot \hat{i}^n) \right) \overline{r}_j^n \cdot \hat{i}^n = \left\| \overline{r}_j^n \right\|^2 \overline{N}_j^n \hat{i}^n \Delta \overline{V}_{C_{j,x}}^{t+1} = \\ &= \frac{\overline{N}_j^n \Delta t}{m_j} + \frac{\overline{N}_j^n \Delta t}{I_j} \left(\left\| \overline{r}_j^n \right\|^2 - (\overline{r}_j^n \cdot \hat{i}^n)^2 \right) = \overline{N}_j^n \Delta t \left(\frac{1}{m_j} + \frac{\left\| \overline{r}_j^n \right\|^2 - (\overline{r}_j^n \cdot \hat{i}^n)^2}{I_j} \right) \end{aligned} \quad (21)$$

A similar approach is used for the \hat{y} component $\Delta \overline{V}_{C_{j,y}}^{t+1}$, where by applying the distributive property to equation (19) it is possible to rearrange it and obtain an equation similar to (21), as shown below in equation (22). For the computation of change in velocity in \hat{j}^n it is considered the equation with both force components ($\overline{T}_j^n + \overline{N}_j^n$), and thus it is obtained an additional term that depends on the \overline{N}_j^n force.

$$\begin{aligned} \Delta \overline{V}_{C_{j,y}}^{t+1} &= \frac{\overline{T}_j^n}{m_j} \Delta t + \frac{\Delta t}{I_j} \left(\left\| \overline{r}_j^n \right\|^2 (\overline{T}_j^n) - (\overline{r}_j^n \cdot \hat{j}^n \left\| \overline{T}_j^n \right\| + \overline{r}_j^n \cdot \hat{j}^n \left\| \overline{N}_j^n \right\|) (\overline{r}_j^n \cdot \hat{j}^n) \right) = \\ &= \frac{\overline{T}_j^n}{m_j} \Delta t + \frac{\Delta t}{I_j} \left(\left\| \overline{r}_j^n \right\|^2 (\overline{T}_j^n) - (\overline{r}_j^n \cdot \hat{j}^n)^2 \overline{T}_j^n - (\overline{r}_j^n \cdot \hat{j}^n) (\overline{r}_j^n \cdot \hat{j}^n) \left\| \overline{T}_j^n \right\| \right) = \\ &= \overline{T}_j^n \Delta t \left(\frac{1}{m_j} + \frac{1}{I_j} \left(\left\| \overline{r}_j^n \right\|^2 - (\overline{r}_j^n \cdot \hat{j}^n)^2 \right) \right) - \frac{\Delta t}{I_j} (\overline{r}_j^n \cdot \hat{j}^n) (\overline{r}_j^n \cdot \hat{j}^n) \left\| \overline{T}_j^n \right\| \hat{j}^n \end{aligned} \quad (22)$$

We also further define E_{xj}^n and E_{yj}^n as the composition between mass, rotational inertia and torque arm of the bodies, as shown by the equation (23). This component can be seen as a value of "effective" mass, and it dictates the resistance to velocity change in the point C^n of the object when a force is applied at that point.

$$\begin{cases} E_{xj}^n = \left(\frac{1}{m_j} + \frac{\left\| \overline{r}_j^n \right\|^2 - (\overline{r}_j^n \cdot \hat{i}^n)^2}{I_j} \right)^{-1} \\ E_{yj}^n = \left(\frac{1}{m_j} + \frac{\left\| \overline{r}_j^n \right\|^2 - (\overline{r}_j^n \cdot \hat{j}^n)^2}{I_j} \right)^{-1} \end{cases} \quad (23)$$

By substituting equation (22) for both objects 1 and 2 in equation (12), we obtain equation (25) that associates the contact force with the change in relative velocity in the \hat{i}^n direction.

$$\Delta \overline{V}_{C_x}^{n+1} = \frac{\overline{N}_1^n \Delta t}{E_{x1}^n} - \frac{\overline{N}_2^n \Delta t}{E_{x2}^n} \quad \overline{N}_1^n = -\overline{N}_2^n \quad \Delta \overline{V}_{C_x}^{n+1} = \Delta t \overline{N}_1^n \frac{(E_{x1}^n + E_{x2}^n)}{(E_{x1}^n E_{x2}^n)} \quad (24)$$

By applying the same approach for the \hat{j}^n direction, the equation (25) is obtained, where for brevity, we define L^n as being the second term of the equation, as shown in equation (25):

$$\begin{aligned} \Delta \overline{V}_{C_y}^{n+1} &= \left(\frac{\overline{T}_1^n \Delta t}{E_{y1}^n} - \frac{\Delta t}{I_1} (\overline{r}_1^n \cdot \hat{j}^n) (\overline{r}_1^n \cdot \hat{j}^n) \left\| \overline{T}_1^n \right\| \hat{j}^n \right) - \left(\frac{\overline{T}_2^n \Delta t}{E_{y2}^n} - \frac{\Delta t}{I_2} (\overline{r}_2^n \cdot \hat{j}^n) (\overline{r}_2^n \cdot \hat{j}^n) \left\| \overline{T}_2^n \right\| \hat{j}^n \right) \\ \overline{T}_1^n &= -\overline{T}_2^n \quad \Delta \overline{V}_{C_y}^{n+1} \\ &= \Delta t \overline{T}_1^n \frac{(E_{y1}^n + E_{y2}^n)}{E_{y1}^n E_{y2}^n} + \Delta t \left\| \overline{N}_1^n \right\| \left(\frac{1}{I_2} (\overline{r}_2^n \cdot \hat{j}^n) (\overline{r}_2^n \cdot \hat{j}^n) - \frac{1}{I_1} (\overline{r}_1^n \cdot \hat{j}^n) (\overline{r}_1^n \cdot \hat{j}^n) \right) \hat{j}^n \\ &= \Delta t \overline{T}_1^n \frac{(E_{y1}^n + E_{y2}^n)}{E_{y1}^n E_{y2}^n} + L^n \end{aligned} \quad (25)$$

And by substituting equations (24) and (25) in the criterion equation (11) we finally obtain equation (26), where the maximum contact force for both directions is obtained. The normal and parallel forces calculated by equations (3) and (8) are limited to the maximum value obtained from equation (26). The forces for object 2 can be obtained by considering that they are the reaction forces of \overline{T}_1^n and \overline{N}_1^n .

$$\begin{cases} \Delta t \overline{N}_1^n \frac{(E_{x1}^n + E_{x2}^n)}{E_{x1}^n E_{x2}^n} \leq \overline{V}_{C_x}^n - \gamma \overline{V}_{C_x}^0 \Rightarrow \overline{N}_1^n \leq \frac{1}{\Delta t} (\overline{V}_{C_x}^n - \gamma \overline{V}_{C_x}^0) \frac{(E_{x1}^n E_{x2}^n)}{(E_{x1}^n + E_{x2}^n)} \\ \Delta t \overline{T}_1^n \frac{(E_{y1}^n + E_{y2}^n)}{E_{y1}^n E_{y2}^n} + J^n \leq \overline{V}_{C_y}^n - \gamma \overline{V}_{C_y}^0 \Rightarrow \overline{T}_1^n \leq \frac{1}{\Delta t} (\overline{V}_{C_y}^n - \gamma \overline{V}_{C_y}^0 - L^n) \frac{(E_{y1}^n E_{y2}^n)}{(E_{y1}^n + E_{y2}^n)} \end{cases} \quad (26)$$

4 VALIDATION

We have evaluated the performance of the Contact Engine in two experiments, in the first one simulations run with integration time-steps varying from 0.1s to 2.0s for both the Contact Engine and the numerical engine are evaluated. In the second experiment the relative velocity of the bodies at the start of the simulation is varied from 0.5 knot to 4.0 knots.

For those evaluations it was considered a scenario with two vessels as objects as depicted in Figure 5. The object 1 is a container vessel 298m long with 46m beam, 9m draft and displacement 87.800 tons. The object 2 is a tugboat 32m long with 13m beam and displacement 930 tons. The object 2 starts the simulation with zero velocity and object 1 starts with a velocity of 4 knots ahead. The objects are 4m apart at the start of simulation

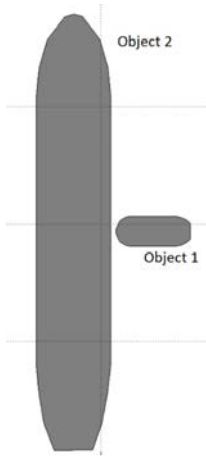


Figure 8. Initial condition for the experimental test. Object 1 and 2 are separated by 1.7m.

The simulations are run in a steady sea, without environmental conditions (wind, waves and currents), and relative velocities between objects and the normal contact forces are written to a text report. As an example we have used the parameters with values defined on Table 1. But it is worthwhile to point that those parameters can be configured to represent the properties of specific fenders if needed.

Table 1. Parameters used for the contact between objects in the experimental setup.

Variable	Value
K	500 kN/m ²
C	0 kN.s/m
K_s	3000 kN/m
μ_s	0.5
μ_k	0.5
γ	0.1
Δt (1st experiment)	[0.1,0.5,1.0,2.0] s
Δt (2nd experiment)	0.1 s

The results for contact normal forces are shown in Figure 9, where it is possible to notice that smaller time-steps produce higher forces with shorter durations, while larger time-steps produce a smaller force distributed over a longer period. This behaviour is expected since the Impulse-Momentum criterion enforces that the integral of force and time is kept the same independent of the time-step length used in the numerical engine.

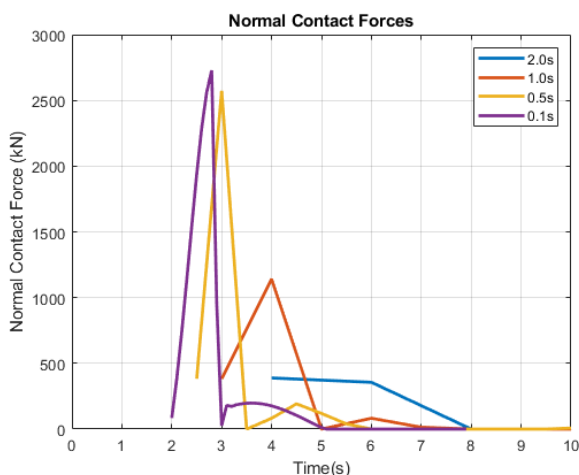


Figure 9. Normal contact forces produced in the experimental setup for varying integration time-steps.

Also is possible to notice in Figure 9 that as the time-step decreases the force peaks tend to converge to a value (eg. the difference between peaks for 0.5s and 0.1s Δt is smaller than the difference between peaks for 0.5s and 1.0s Δt) since the discretized model tends to approach the true solution as the time-step length is shortened.

The relative velocity between objects is shown in Figure 10. It is possible to notice that for all time-steps, the Contact Engine produced similar results, with objects ending the contact with a residual velocity that is similar to the expected theoretical value. The only notable difference is that for larger time-steps the contact takes longer and the relative velocity converges slower to the expected value.

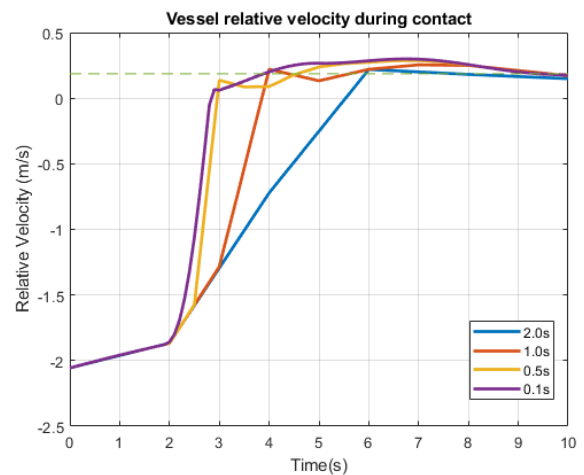


Figure 10. Relative velocities between objects during the contact. The dotted line is the final velocity expected by the equation (10).

To evaluate the effect of initial relative velocity, the same scenario was used for the second experiment, but the initial velocity of object 2 was modified between 0.5 knot and 4 knots and the distance between vessels has been reduced to 2 meters, and thus the results in Figure 11 were obtained, where it is possible to notice that the same behaviour is obtained for different contact speeds.

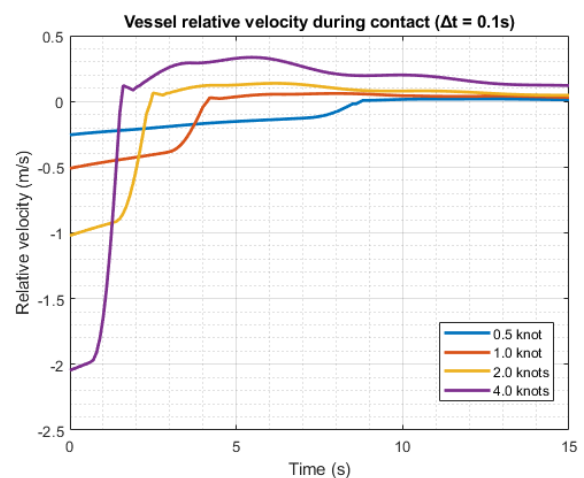


Figure 11. Relative velocities between objects during the contact for different initial velocities for the body 2.

The forces during the contact also behave as expected, with smaller peak forces for collision with

lower velocity between the vessels. The duration of the first contact forces peak also slightly increases for contacts in lower velocities, having a duration between 1 and 2 seconds. It is also relevant to notice that the intersection between vessel polygons is kept small for all the contact velocities, as shown in table 2, having a maximum penetration between geometries of 0.97m for the 4 knots scenario.

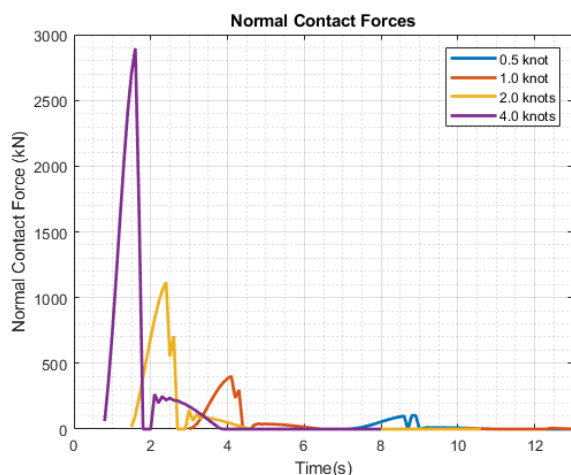


Figure 12. Contact forces for scenarios with different relative velocities between objects.

Table 2. Maximum penetration between vessels' polygons.

Initial velocity	Maximum depth
4.0 knots	0.96 m
2.0 knots	0.53 m
1.0 knot	0.29 m
0.5 knot	0.14 m

5 CONCLUSIONS

In this paper, a 2D time-discretized model for contact forces between bodies was presented. Its performance was evaluated by comparing its behaviour for varying integration time-steps duration in a numerical manoeuvring simulator. The contact model performs close to the expected, considering the hypothesis adopted in its formulation, even for large integration time-steps.

The model considers both restoration forces and friction forces between bodies. The model is simplified, so it can be run in Real-Time simulations, and can be satisfactorily used for cases where the dynamical behaviour of the bodies in the simulation is more important than the accurate computation of peak values or contact forces.

As further steps for improving the model, one possibility is to run high-resolution Finite Element

Analysis of the contact between typical marine fenders and ship hulls, and use it as a gold standard to compare to the model proposed. A direct comparison between the forces calculated by both models will provide a way to objectively measure the performance of the proposed model, and it might give insight into where the model could be improved.

ACKNOWLEDGMENTS

The authors acknowledge ANP/Petrobras for sustaining long-term support in the development of the Ship Maneuvering Simulator Center (SIGITEC 2018/00402-5). The first and last authors also thank the Center for Artificial Intelligence (C4AI-USP), supported by the São Paulo Research Foundation and by the IBM Corporation (FAPESP grants 2019/07665-4 and 2020/16746-5). The last author acknowledges the CNPq – Brazilian National Council for Scientific and Technological Development for the research grants (process 310127/2020-3).

REFERENCES

- [1] PIANC (2002), Guidelines for the Design of Fender Systems: 2002, report of working group 33 of the Maritime Navigation Commission, Brussels.
- [2] Antoloni, G., Carbonari, S., Gara, F., Lorenzoni, C. and Mancinelli, A. (2017). 'Simple Physical Models to Simulate the Behavior of Buckling-Type Marine Fenders', Journal of Waterway, Port, Coastal, and Ocean Engineering, vol. 143, no. 1, p. 04016014.
- [3] Eskew, Z., (2020). "A Computational Analysis of Marine Fenders Under Heavy Weather Mooring Conditions" (2020). UNF Graduate Theses and Dissertations. 997. Retrieved from: <https://digitalcommons.unf.edu/etd/997>
- [4] Han, Z., Li, C., Deng, Y. and Liu, J. (2019). "The analysis of anti-collision performance of the fender with offshore wind turbine tripod impacted by ship and the coefficient of restitution". Ocean Engineering. Volume 194, p. 106614, ISSN 0029-8018, <https://doi.org/10.1016/j.oceaneng.2019.106614>.
- [5] Atiq, M.S., Shajib, A.K.J. Hoquem K.N., (2022). "Analysis of Marine Fender Systems Minimizing the Impact of Collision Damage". Proceedings of MARTEC 2022, The International Conference on Marine Technology, Dhaka, Bangladesh
- [6] Tannuri, E. A., Rateiro, F., Fucatu, C. H., Ferreira, M. D., Masetti, I. Q., & Nishimoto, K., (2014), "Modular mathematical model for a low-speed maneuvering simulator". In International Conference on Offshore Mechanics and Arctic Engineering, ASME-OMAE, San Francisco, USA.
- [7] Gea-Banaclache, J. (2019). "University Physics I: Classical Mechanics". Open Educational Resources. Retrieved from <https://scholarworks.uark.edu/oer/3>
- [8] Likharev, Konstantin, "Part CM: Classical Mechanics" (2013). Essential Graduate Physics. 2. Retrieved from <https://commons.library.stonybrook.edu/>